JACS
JOURNAL OF THE AMERICAN CHEMICAL SOCIETY
Article
pubs.acs.org/JACS

Pressure-Driven Cooperative Spin-Crossover, Large-Volume Collapse, and Semiconductor-to-Metal Transition in Manganese(II) Honeycomb Lattices

Yonggang Wang,[*,†,‡,▼] Zhengyang Zhou,[§,∥,▼] Ting Wen,[⊥] Yannan Zhou,[⊥] Nana Li,[#] Fei Han,[‡,#,¶] Yuming Xiao,[△] Paul Chow,[△] Junliang Sun,[§] Michael Pravica,[†] Andrew L. Cornelius,[†] Wenge Yang,[*,‡,#] and Yusheng Zhao[*,†,▲]

[†]High Pressure Science and Engineering Center, University of Nevada, Las Vegas, Nevada 89154, United States
[‡]HPSynC, Geophysical Laboratory, Carnegie Institution of Washington, Argonne, Illinois 60439, United States
[§]College of Chemistry and Molecular Engineering, Peking University, Beijing 100871, China
[∥]College of Chemistry and Chemical Engineering, Chongqing University, Chongqing 400044, China
[⊥]Institute of Nanostructured Functional Materials, Huanghe Science and Technology College, Zhengzhou, Henan 450006, China
[#]Center for High Pressure Science and Technology Advanced Research (HPSTAR), Pudong, Shanghai 201203, China
[¶]Center for the Study of Matter at Extreme Conditions, Department of Mechanical and Materials Engineering, Florida International University, Miami, Florida 33199, United States
[△]High Pressure Collaborative Access Team (HPCAT), Geophysical Laboratory, Carnegie Institution of Washington, Argonne, Illinois 60439, United States
[▲]Southern University of Science and Technology, Shenzhen 518055, China

Supporting Information

ABSTRACT: Spin-crossover (SCO) is generally regarded as a spectacular molecular magnetism in $3d^4$–$3d^7$ metal complexes and holds great promise for various applications such as memory, displays, and sensors. In particular, SCO materials can be multifunctional when a classical light- or temperature-induced SCO occurs along with other cooperative structural and/or electrical transport alterations. However, such a cooperative SCO has rarely been observed in condensed matter under hydrostatic pressure (an alternative external stimulus to light or temperature), probably due to the lack of synergy between metal neighbors under compression. Here, we report the observation of a pressure-driven, cooperative SCO in the two-dimensional (2D) honeycomb antiferromagnets $MnPS_3$ and $MnPSe_3$ at room temperature. Applying pressure to this confined 2D system leads to a dramatic magnetic moment collapse of Mn^{2+} (d^5) from $S = 5/2$ to $S = 1/2$. Significantly, a number of collective phenomena were observed along with the SCO, including a large lattice collapse (~20% in volume), the formation of metallic bonding, and a semiconductor-to-metal transition. Experimental evidence shows that all of these events occur in the honeycomb lattice, indicating a strongly cooperative mechanism that facilitates the occurrence of the abrupt pressure-driven SCO. We believe that the observation of this cooperative pressure-driven SCO in a 2D system can provide a rare model for theoretical investigations and lead to the discovery of more pressure-responsive multifunctional materials.

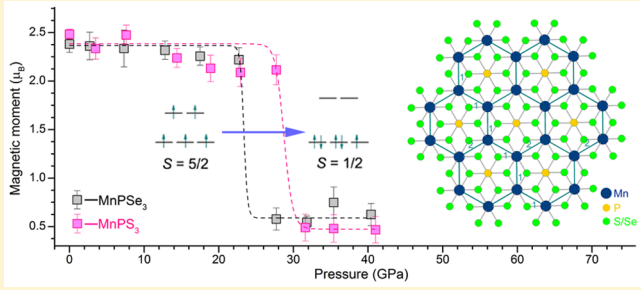

INTRODUCTION

Spin-crossover (SCO), as a spin-state transition behavior of transition metal compounds initiated by external stimuli such as light, heat, pressure, and magnetic fields, has attracted intense interest for exploring materials with novel structural and physical properties.[1−6] This intriguing phenomenon is typically observed in the first-row d^4–d^7 transition metal complexes, where the metal ion centers exhibit the ability to undergo an electronic configuration switch between high-spin (HS) and low-spin (LS) states when the outer environment changes. According to crystal-field theory, whether or not a transition metal ion embedded in the crystalline matrix will have a HS or LS electron configuration is determined by the magnitude of the crystal-field splitting energy ($\Delta = 10Dq$) along with the Hund's intra-atomic exchange energy (J).[7,8] Accordingly, an important principle for exploring new SCO materials is selecting suitable organic ligands and constructing them with

Received: September 29, 2016
Published: November 14, 2016

DOI: 10.1021/jacs.6b10225
J. Am. Chem. Soc. 2016, 138, 15751−15757

transition metal ions into cooperative networks, where the energy levels in Δ and J are close enough to be driven by temperature or light irradiation and generate crossover. Besides the doubtlessly significant and fundamental aspects of SCO, one of its most interesting features is that the electronic and/or magnetic interactions between transition metal neighbors often give rise to other remarkable cooperative phenomena such as memory effect, first-order structural transition, metal-insulator transition, and long-range magnetic ordering.[9−11] This also makes SCO materials promising for multifunctional applications. However, it is worth noting that, until now, most of the SCO phenomena have been reported in soft materials, such as organic−inorganic hybrid complexes,[1−3,5,12−15] and the frequently implemented external stimuli are light and temperature. Exploring SCO in more inorganic materials, especially in strongly correlated systems, is still a great challenge due to the difficulty of changing the strong inorganic bonds (*e.g.*, ionic and covalent bonding).

Pressure, as an alternative external stimulus to light or thermal excitation, is an efficient tool for altering crystal-field strength by shortening the metal−ligand bond lengths and thus has promise to drive SCO in strongly correlated systems. Recent reports include the SCO in magnesiowüstite (Mg,Fe)-O,[16−18] silicate perovskites $(Mg,Fe)(Si,Al)O_3$,[19] and magnetite Fe_3O_4,[20] which provided in-depth understanding of the concurrent structural and electronic anomalies and seismic-wave heterogeneity in the Earth's lower mantle. In other examples, such as YCo_5,[21] MnO,[22] FeS,[23] and $SrFe(II)O_2$,[24] SCO was observed accompanying lattice collapse and Mott transitions, etc. However, considering that pressure has a gradual effect on the interatomic distance and band gap, pressure-induced SCO often represents a progressive process. Thus, they are not as sharp as those in the light- or temperature-induced SCO processes associated within molecular complexes or theoretical calculations.[25−28] This drawback greatly hinders harnessing pressure-induced SCO for potential applications in sensors or memory devices.

Our aim is to initiate and observe instantaneous SCO from high-level spins to low-level spins. Inspired by the light- and temperature-induced SCO in metal−organic complexes at ambient pressure,[29,30] where an abrupt spin change indicates a remarkable "cooperative behavior" between neighboring metal centers, a rational strategy to cause abrupt pressure-driven SCO is to introduce "cooperativity". As is known, application of pressure may lead to not only SCO but also metal ionic radii and orbital repopulation collapses. This sometimes leads to other abrupt changes like the large volume collapse of more than 20% in MnS_2 and MnS.[31,32] If these behaviors can, in turn, assist the occurrence of SCO and they occur synergistically, then an abrupt pressure-driven SCO is anticipated. In the search for materials with such behavior, we have studied the SCO behavior of MnS and MnSe under compression.[33] The spin-state transition coupled with giant lattice collapses and accompanied the formation of intermetallic bonding, which leads to a semiconductor-to-metal transition (Mott transition). However, the SCO process still occurs somewhat progressively, which might be attributed to the three-dimension (3D) structural construction from the low-pressure rocksalt phase to the high-pressure MnP-type structure. For comparison, a low-dimensional confined system would be more promising to achieve the proposed synergistic effect with less constraint from the third dimension.

In this article, we report the first successful account of pressure-induced spin-state transitions in the two-dimensional (2D) honeycomb compounds $MnPS_3$ and $MnPSe_3$. An abrupt SCO from HS to LS electronic configurations was observed in both materials around 25−30 GPa. In situ high-pressure structural and transport characterizations show that the sharp pressure-driven SCO accompanies large in-plane lattice collapse and a semiconductor-to-metal transition. Based on this experimental evidence, we give clear instructions to achieve cooperative pressure-driven SCO materials.

EXPERIMENTAL DETAILS

Sample Preparation. $MnPS_3$ and $MnPSe_3$ powders were synthesized by reacting stoichiometric Mn, P, and S powders at 700 °C in a sealed quartz tube for several days. The $MnPS_3$ sample appeared greenish and had a single-crystalline sheet form. The $MnPSe_3$ sample was a dark red powder. The phase purity of each synthesized sample was confirmed by X-ray diffraction (XRD) at room temperature and ambient pressure.

In Situ High-Pressure Characterizations. For the in situ high-pressure measurements, a symmetric diamond anvil cell (DAC) was employed to generate high pressure. Steel gaskets were preindented to a thickness of 40 μm followed by laser drilling the central part to form a 120 μm diameter hole which served as the sample chamber. Precompressed $MnPS_3$ and $MnPSe_3$ pellets and ruby balls were loaded in the gasket holes in separate experiments. Silicone oil was used as the pressure-transmitting medium (PTM), and the pressures were determined using the ruby fluorescence method.[34] The in situ synchrotron XRD experiments were conducted at the 16 BM-D station of the High-Pressure Collaborative Access Team (HPCAT) at the Advanced Photon Source of Argonne National Laboratory (ANL). A focused monochromatic X-ray beam about 5 μm in diameter (fwhm) and 0.3066 Å wavelength was used for the diffraction experiments. The diffraction data were recorded by a MAR345 image plate. For the high-pressure X-ray emission spectra (XES) experiments performed at the 16 ID-D station of HPCAT, Be gaskets were used as the sample chamber and silicone oil was used as the PTM. Raman spectra were recorded with a Raman spectrometer with a 532.1 nm laser located at the High Pressure Synergetic Consortium (HPSynC) at the APS.

In situ high-pressure electric resistance was measured by a four-point-probe resistance measurement system consisting of a Keithley 6221 current source, a 2182A nanovoltmeter, and a 7001 voltage/current switch system at HPSynC. A thin cubic boron nitride layer was inserted into the DAC between the steel gasket and diamond anvil to provide electrical insulation between the electrical leads and gasket. Four gold wires were arranged to contact the sample in the chamber for resistance measurements.

Data Analyses. The XRD patterns were integrated into one-dimensional profiles using the Dioptas program.[35] Le Bail fitting was performed using the FULLPROF program.[36] The quantitative analyses of the XES data were conducted using the integral of the absolute values of the difference spectra (IAD method).[37]

RESULTS AND DISCUSSION

Pressure-Driven SCO. $MnPS_3$ and $MnPSe_3$ are regarded as examples of 2D Heisenberg-like antiferromagnets with magnetic Mn^{2+} ions arranged in a nearly perfect honeycomb lattice.[38,39] Previous studies have mainly focused on their magnetism and chemical intercalations,[40−43] but very few high-pressure-related investigations have been performed on them or on similar honeycomb systems until now.[44,45] Their crystal structures consist of a succession of sandwiches along the c-axis. Each sandwich is composed of two layers of S or Se atoms which have octahedrally coordinated Mn^{2+} ions and phosphorus pairs in the ratio of 2:1. As the repeating sandwiches are weakly bonded via van der Waals interactions, superexchanging

DOI: 10.1021/jacs.6b10225
J. Am. Chem. Soc. 2016, 138, 15751−15757

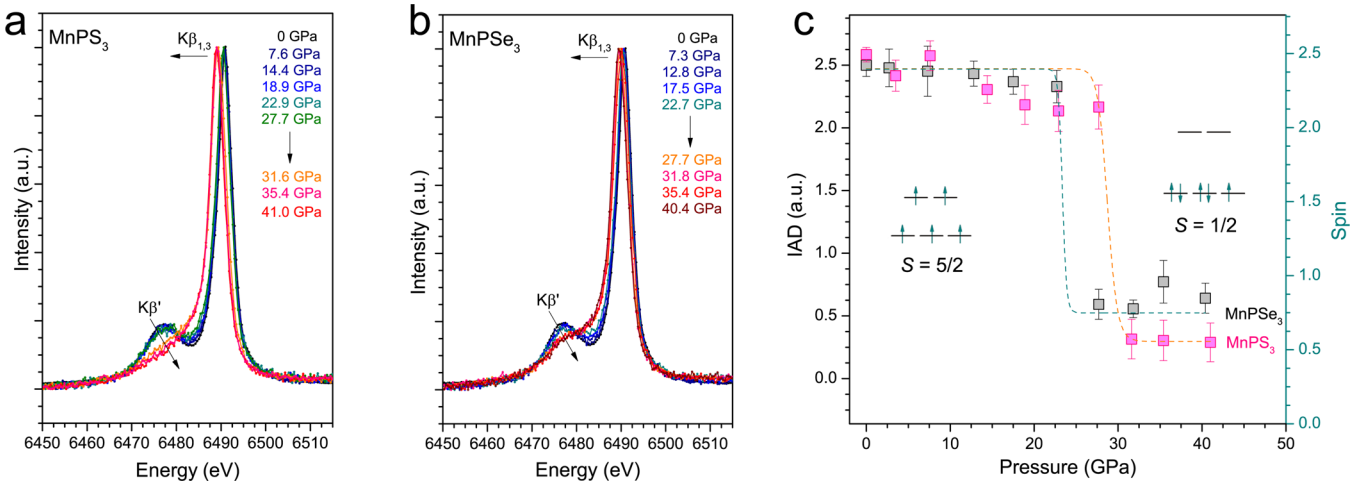

Figure 1. Mn K_β XES of (a) $MnPS_3$ and (b) $MnPSe_3$ as a function of applied pressures. (c) IAD and spin values as a function of pressure, obtained relative to the ambient spectra of $MnPS_3$ and $MnPSe_3$.

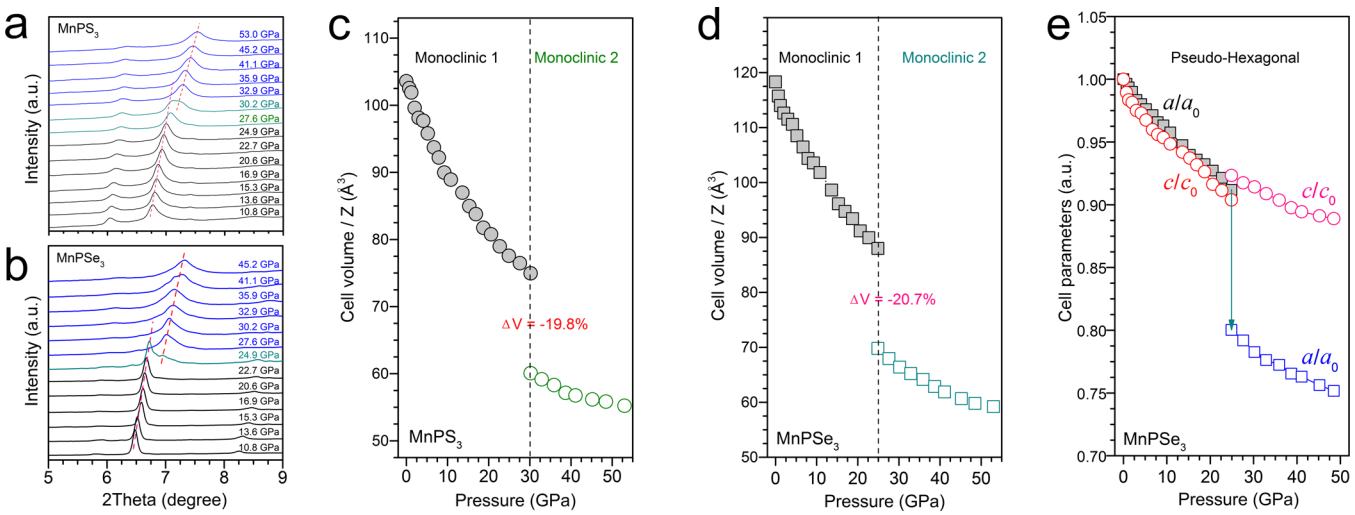

Figure 2. Position changes of (a) (131) and $(20\bar{2})$ peaks for $MnPS_3$ and (b) (113) peak for $MnPSe_3$ under compression. (c) Experimental cell volumes as a function of applied pressure for the LP and HP phases of $MnPS_3$. (d) Experimental cell volumes as a function of applied pressure for the LP and HP phases of $MnPSe_3$. (e) Cell parameters of $MnPSe_3$ as a function of pressure showing anisotropic compressibility.

pathways between the honeycomb layers can be ruled out. In our previous studies of MnS and MnSe,[33] we proposed that the pressure-induced SCO, accompanied by lattice collapse and the formation of intermetallic bonding, should be a universal behavior in manganese chalcogenides. Thus, $MnPS_3$ and $MnPSe_3$ are ideal candidates, as low-dimensional confined systems, for realizing cooperative pressure-driven SCO.

XES studies[23,46] combined with XRD and transport measurements on ~50 μm sized samples confined inside DACs were performed to study the spin state and structural and transport behaviors under high pressure, respectively. Figure 1a,b presents the Mn $K\beta$ XES spectra of $MnPS_3$ and $MnPSe_3$ under compression up to 41 GPa, respectively. All spectra comprise a main $K\beta_{1,3}$ peak located around 6490 eV and a satellite $K\beta'$ peak located around 6478 eV. As is known, the $K\beta$ emission lines are characteristic X-ray emissions originating from the 3p → 1s decay. The shape of the $K\beta$ emission line is determined by the final state interactions between the 3p core hole and the partially filled 3d shell electrons.[23] Thus, one can qualitatively distinguish the HS-to-LS state transition from the decrease in the intensity of the satellite peak $K\beta'$ and the peak position of $K\beta_{1,3}$. In the low-pressure range (0–27.7 and 0–22.7 GPa for $MnPS_3$ and $MnPSe_3$, respectively), well-defined $K\beta'$ satellite peaks are observed for both $MnPS_3$ and $MnPSe_3$, indicating a HS ground state ($S = 5/2$). The Mn $K\beta'$ peaks decrease suddenly with an increase in pressure, exceeding 31.6 GPa for $MnPS_3$ and 27.7 GPa for $MnPSe_3$. Correspondingly, the Mn $K\beta_{1,3}$ lines shift to lower energy sides. This evidence indicates the occurrence of pressure-driven SCO of Mn^{2+} in the honeycomb lattice, that is, from the HS state to the LS state. Notably, judging from the XES data visually, the spin-state changes are abrupt rather than gradual like almost of all the previously reported examples of pressure-driven SCO.

To illustrate the pressure-driven SCO in $MnPS_3$ and $MnPSe_3$ more clearly, quantitative analysis of the XES data following the procedure described by Vankó et al.[37] was conducted with the IAD method. All of the XES spectra were normalized first with respect to the area under the curves and then shifted to have centers of mass at the same position. The differential curves are shown in Figure S1. In this situation, the IAD value reflects a linear relationship with the average spin numbers. Figure 1c

DOI: 10.1021/jacs.6b10225
J. Am. Chem. Soc. 2016, 138, 15751–15757

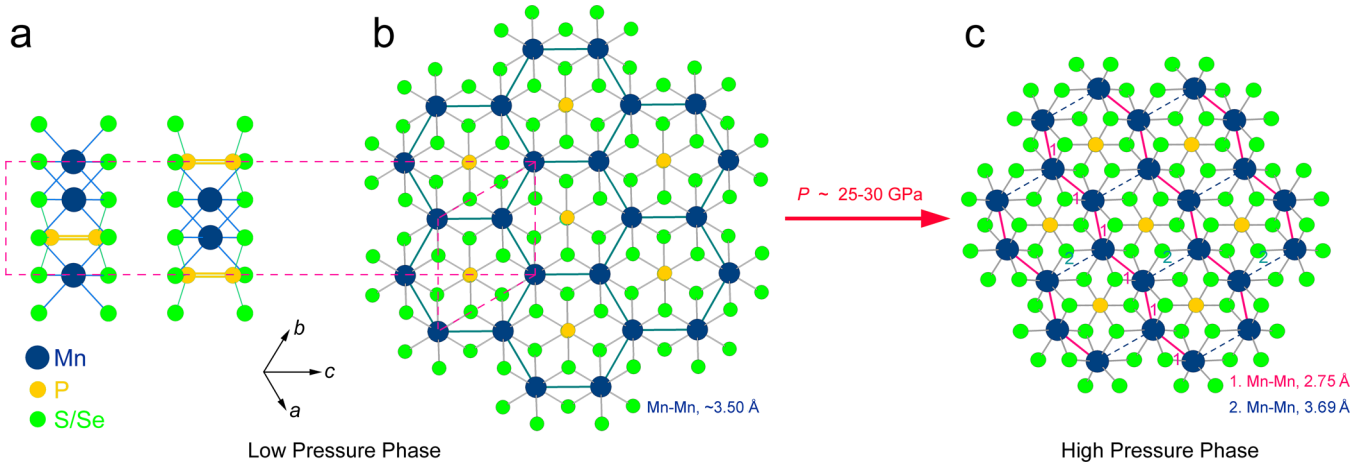

Figure 3. Crystal structures for the low-pressure phase of $MnPS_3$ and $MnPSe_3$ (a) viewed along the *a*-axis showing the layered structure feature and (b) viewed along the *c*-axis showing the Mn^{2+} honeycomb lattice. (c) Proposed high-pressure structure for $MnPS_3$ and $MnPSe_3$. The shortest or the near-shortest Mn−Mn bond lengths are highlighted by pink and blue lines. The schematic Mn−Mn bond length values are taken from the $MnPS_3$ structures at ambient conditions and at 32.9 GPa, respectively.

shows the pressure dependence of the Mn^{2+} spin values in $MnPS_3$ and $MnPSe_3$ from the IAD analysis. The starting materials at ambient conditions are considered to have a HS electronic configuration for Mn^{2+} with $S = 5/2$ (IAD = 0). Below the pressure thresholds of the SCO, the IAD value remains almost unchanged at 5/2. When the applied pressure exceeds the value for causing the SCO, the IAD value drops to the $S = 1/2$ LS state level abruptly, indicating a complete collapse of the Mn^{2+} moments in both materials. There are still some residual spins for $MnPSe_3$, that is, the IAD value is a little more than 1/2. The exact reason for this is still unknown. We attribute the abrupt pressure-driven SCO phenomenon in $MnPS_3$ and $MnPSe_3$ to their 2D crystal structures, where the magnetic spins located on the confined Mn honeycomb lattice are expected to accommodate neighboring spins more collectively than in other 3D crystalline materials.[16−20,23]

Large Pressure-Driven In-Plane Lattice Collapse. To confirm if there is a dramatic structural change involved in the abrupt pressure-driven SCO, we studied the crystal structure evolution by in situ high-pressure XRD measurements. The XRD patterns of $MnPS_3$ and $MnPSe_3$ as a function of pressure up to 53.0 GPa are shown in Figure S2. Figure 2a,b zooms in on the distinguishing discontinuous shift and splitting of the main diffraction peaks located at $2\theta = 6-7°$ (Miller index = $(113)/(20\bar{2})$ for $MnPS_3$ and (113) for $MnPSe_3$, respectively), which indicate synchronous abrupt lattice shrinkage and SCO in response to external pressure. Despite the different crystalline symmetries, $C2/m$ for $MnPS_3$ and $R\bar{3}$ for $MnPSe_3$, they adopt nearly the same corresponding crystal structures before and after the transition, based on the analyses of diffraction data.[38,39] We were unable to determine the exact structures of the high-pressure phases (symmetry and atomic positions) due to the low quality of the high-pressure XRD patterns. Instead, Le Bail fitting analyses were conducted to help us to understand the structural changes. From the XRD patterns, an isostructural or quasi-isostructural phase transition is very likely for both $MnPS_3$ and $MnPSe_3$. Thus, monoclinic unit cells with space group $C2/m$ were adopted for cell parameter fitting for $MnPS_3$ and $MnPSe_3$ (Figure S3), and the trigonal space group $R\bar{3}$ was adopted for the analyses of anisotropic compressibility of $MnPSe_3$ for simplicity.

Figure 2c,d displays the cell volumes of $MnPS_3$ and $MnPSe_3$ versus applied pressures. Dramatic cell volume decreases (−19.8 and −20.7% for $MnPS_3$ and $MnPSe_3$, respectively) from the low-pressure phases to the high-pressure phases dominate the $P-V$ profiles, indicating the occurrence of first-order phase transitions with substantial changes in their atomic arrangement. As even a 5% volume collapse in any other material during a phase transition has been regarded as significant,[22,31,47−49] such giant pressure-driven lattice collapses are novel and may originate from the pressure-driven SCO. The decrease of Mn^{2+} ionic sizes during the SCO from 0.83 Å (HS) to 0.67 Å (LS)[50] will inevitably act on the Mn−(S/Se) bond lengths and also possibly lead to the symmetry-breaking of the honeycomb lattice into denser phases. In Figure 2e, an anisotropic compressibility behavior during the phase transition is clearly observed in $MnPSe_3$, which indicates that the volume collapses are from the abrupt shrinkage of the honeycomb lattice (*ab*-plane) rather than perpendicular to the honeycomb layer (*c*-axis). This evidence points to the formation of in-plane metallic bonding between the Mn^{2+} centers.

Crystal Structure Evolution and the Formation of Metallic Bonding. Figure 3a,b displays the crystal structures of the low-pressure phases of $MnPS_3$ and $MnPSe_3$ (the slight distortion of $MnPS_3$ from the trigonal symmetry is disregarded here). Viewed perpendicularly to the *c*-axis, we can see the well-separated sandwich layers associated with weak interlayer van der Waals forces. All Mn atoms coordinate with six S/Se atoms, and the $Mn(S,Se)_6$ octahedra share their edge with three neighbors to form the honeycomb lattice, with $P_2(S/Se)_6^{4-}$ groups located in the center of the six-fold mesh. The shortest Mn−Mn distance in $MnPS_3$ is approximately 3.50 Å at ambient conditions. As discussed, the shrinkage of the honeycomb layer contributes most to the volume collapse along with the SCO. This poses an interesting question: is the in-plane lattice collapse isotropic or anisotropic? Taking $MnPS_3$ as an example, in the first situation, a compressed honeycomb lattice forms with the shortest Mn−Mn distances of about 3.10 Å, which is not short enough to form metal−metal bonding and cannot explain the abrupt SCO phenomenon. Theoretically, the volume collapse from an isostructural phase transition of $MnPS_3$ with only HS-to-LS transitions of Mn^{2+} should give only ~12.2%, which is much less than the experimental

DOI: 10.1021/jacs.6b10225
J. Am. Chem. Soc. 2016, 138, 15751−15757

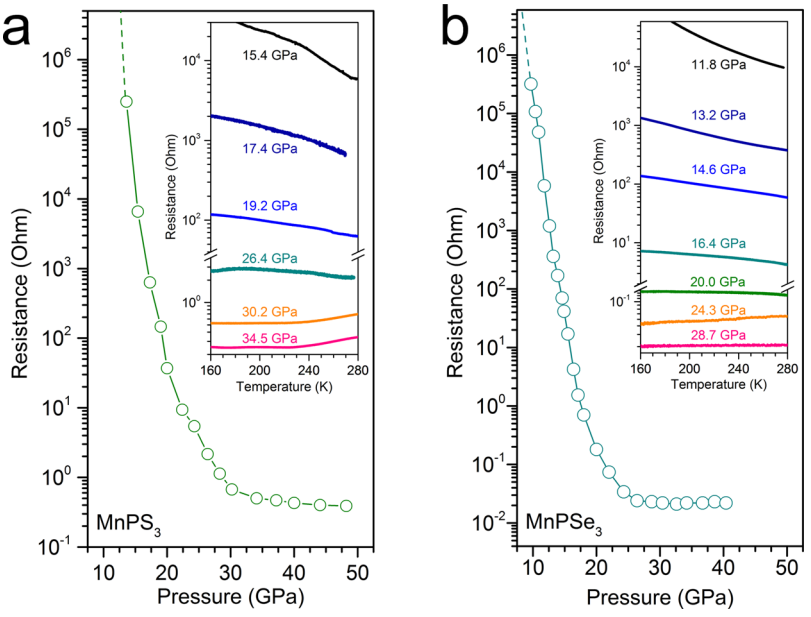

Figure 4. Electrical resistances of (a) $MnPS_3$ and (b) $MnPSe_3$ as a function of pressure show the semiconductor-to-metal transition. Insets of a and b show the temperature dependence ($R-T$) of the resistance of $MnPS_3$ and $MnPSe_3$ under high pressure, respectively.

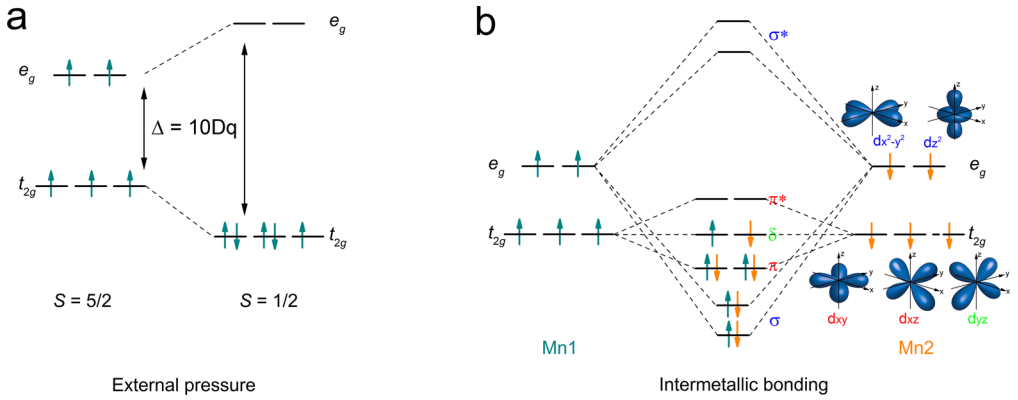

Figure 5. Schematic illustration of the SCO initiated by (a) pure pressure effect and (b) formation of Mn−Mn intermetallic bonding.

observation. In the second case, the trigonal symmetry is broken and the Mn−Mn bonds split into two groups: a metallic bond with a Mn−Mn distance of 2.75 Å and an elongated Mn−Mn distance of 3.69 Å, as shown in Figure 3c. The formation of metallic Mn−Mn bonds is considered to be the most incidental event during the giant pressure-driven lattice collapse and favors the dramatic magnetic moment collapse well. The formation of Mn−Mn metallic bonds is also supported by Raman spectroscopic evidence as all Raman peaks disappear beyond the SCO pressure point (Figure S4) since the possibility caused by symmetry changes can be ruled out.

It is interesting to compare the metallic bonds in high-pressure phases of $MnPS_3$ and $MnPSe_3$ with those in the high-pressure phases of MnS/MnSe[33] and MnS_2.[31] The high-pressure phase of MnS/MnSe adopts a MnP-type structure, where all of the Mn atoms are connected by Mn−Mn metallic bonding to form a three-dimensional network and an obvious metallic transport behavior is observed. In the case of MnS_2, it is reported that Mn−Mn metallic bonds form dimers to stabilize the HP structure and the semiconductor character is preserved in the high-pressure phase. However, in the cases of $MnPS_3$ and $MnPSe_3$, the quasi-one-dimensional Mn(II) chains via metallic Mn−Mn bonds form in the honeycomb lattice, for which an anisotropic transport behavior or a half-metal feature is expected.

Pressure-Induced Semiconductor-to-Metal Transition. In situ transport property measurements were performed to validate the formation of the Mn−Mn metallic bonds in the honeycomb lattice. Figure 4 shows the results of electrical resistance measurements of $MnPS_3$ and $MnPSe_3$ as functions of pressure and temperature. Below 10 GPa, the resistances of both $MnPS_3$ and $MnPSe_3$ are too high to be detected, representing insulating behaviors. Along with the pressure increases, the resistance curves drop quickly by more than 5 orders of magnitude and are followed by a critical point around 25−30 GPa for both materials. The tendencies of the $R-T$ plots indicate a semiconductor-to-metal transition along with the structural and spin-state transitions. However, since we have speculated that the Mn−Mn metallic bonding only exists in the honeycomb plane and even in a quasi-one-dimensional manner, the high-pressure phases should exhibit the semi-metallic transport behavior measured in powder forms. Experimentally, this idea is supported by two phenomena: first, after the phase transition, the electric resistance remains a

DOI: 10.1021/jacs.6b10225
J. Am. Chem. Soc. 2016, 138, 15751−15757

"bad" metal or semimetal; second, in the cooling process, the resistance of the two materials decreases first and then remains nearly constant, indicating the participation of thermally excited carriers contributing to the electrical transport.

$MnPS_3$ and $MnPSe_3$ are new examples of condensed matter with simultaneous SCO, lattice collapse, and semiconductor-to-metal transition. The most important result is that all of these three phenomena occur concurrently and synergistically. During the process, pressure is the critical driving force and the three pressure-driven events are the responses to pressure but assist the onset of each other. Previously, we proposed that the key role for achieving a pressure-driven SCO was the selection of suitable 3d transition metal ions and heavy p-element ligands such as S, Se, and Te.[33] Now, an additional instruction to pursue cooperative pressure-driven SCO is to accommodate the above-mentioned elements into a highly confined crystal lattice, where coupling within the transition metal network should be unimpeded.

Figure 5 presents the ordinary effect of pressure on the electronic configurations of Mn^{2+} compared with the formation of metallic bonding. The spin state of a transition metal ion depends on the competition between the crystal-field splitting energy Δ and Hund's intra-atomic exchange energy J. As it is well-known that external pressure will affect the value of Δ more markedly than J, the ambient high-spin state of Mn^{2+} ($t_{2g}^3e_g^2$, $S = 5/2$) will transform to a low-spin state ($t_{2g}^5e_g^0$, $S = 1/2$) only if the applied pressure is high enough. Such a "pure" pressure effect comes from the enhanced hybridization between the 3d orbital of Mn^{2+} and p orbital of S/Se ligands. Thus, the pressure-driven spin-state transition may occur steadily, as it is normally observed in most condensed matters. When the pressure-driven SCO is coupled with a giant lattice collapse where metallic Mn−Mn bonds form between neighboring Mn atoms, the hybridization between the 3d orbitals will further lower the energies of the bonding orbitals. Two metallic σ bonds ($d(x^2-y^2)$, $d(z^2)$), two π bonds (d_{xy}, d_{xz}), and two δ bonds (d_{yz}) form, and the pairing of the spins leads to a final low-spin state ($S = 1/2$) of Mn^{2+} ions. In this case, the pressure-driven SCO benefits from the hybridization between the 3d orbitals of two neighboring Mn atoms. On the other hand, one can also consider that the formation of Mn−Mn metallic bonding is somehow the result of the dramatic decrease in the Mn^{2+} ionic size from 0.83 Å (HS) to 0.67 Å (LS)[50] and thus reveals the underlying "cooperativity". The visual phenomenon is an abrupt pressure-driven SCO accompanied by a large lattice collapse and the formation of metallic bonding in a condensed solid.

Whether or not pressure-induced SCO is associated with a Mott transition is an essential question in condensed matter research.[23] A confident answer from the viewpoint of structural chemistry and based on our observations is that, a "cooperative" pressure-induced SCO will inevitably couple with the formation of metallic bonding, but the formation of metallic bonding does not equal a metallic transport behavior, which is also dependent on the topology of the metal centers in the crystal structure. An extreme example is pressure-induced SCO with the formation of metal−metal pairs, as proposed in the case of MnS_2,[31] where the high-pressure phase behaves as an insulator. However, this viewpoint still needs to be verified by more experiments. Moreover, the proposed structural models of the high-pressure phases of $MnPS_3$ and $MnPSe_3$ also need to be verified by either further structural evidence (such as pair distribution function or extend X-ray absorption fine structure) or theoretical total energy calculations.

CONCLUSION

In summary, we report a pressure-driven cooperative SCO in the 2D Mn(II) honeycomb antiferromagnets $MnPS_3$ and $MnPSe_3$. The abrupt pressure-driven SCO in these strongly correlated systems is like the thermal- or light-driven SCOs reported in metal−organic complexes at ambient pressure. This can be attributed to the synergistic effect between the pressure-driven SCO, the large lattice collapse, and the semiconductor-to-metal transition. Based on the combined analyses of experimental XRD, XES, and electronic transport data, a concise structural model for the high-pressure phases of $MnPS_3$ and $MnPSe_3$ is proposed to better understand the underlying mechanism. The dimensionality reduction strategy toward the rational design of cooperative pressure-driven SCO in 2D honeycomb lattices not only provides a new pathway to more switching materials that are applicable for sensor and memory devices but also offers a platform to study the fundamental relationship between spin, orbital, lattice, and macroscopic functionalities under pressure.

ASSOCIATED CONTENT

Supporting Information

The Supporting Information is available free of charge on the ACS Publications website at DOI: 10.1021/jacs.6b10225.

IAD analysis results, in situ high-pressure XRD patterns and Raman spectra, and the fitting results of cell parameters, including Figures S1−S4 (PDF)

AUTHOR INFORMATION

Corresponding Authors

*yyggwang@gmail.com
*yangwg@hpstar.ac.cn
*zhaoys@sustc.edu.cn

ORCID

Yonggang Wang: 0000-0003-4816-9182

Author Contributions

▼Y.W. and Z.Z. contributed equally to this work.

Notes

The authors declare no competing financial interest.

ACKNOWLEDGMENTS

This work was supported by National Natural Science Foundation of China (21301063). The UNLV High Pressure Science and Engineering Center (HiPSEC) is a DOE-NNSA Center of Excellence supported by Cooperative Agreement DE-NA0001982. HPCAT operations are supported by DOE-NNSA under Award No. DE-NA0001974 and DOE-BES under Award No. DE-FG02-99ER45775, with partial instrumentation funding by NSF. APS is supported by DOE-BES, under Contract No. DE-AC02-06CH11357. Y.W. thanks Dr. L. Yang and R. Ferry (HPSynC) for their valuable suggestions in the experiments, and Freyja O'Toole (HPSTAR) for her help in language editing.

REFERENCES

(1) Real, J. A.; Gaspar, A. B.; Muñoz, M. C. *Dalton Trans.* **2005**, 2062−2079.

DOI: 10.1021/jacs.6b10225
J. Am. Chem. Soc. 2016, 138, 15751−15757

(2) Gütlich, P.; Garcia, Y.; Goodwin, H. A. *Chem. Soc. Rev.* **2000**, *29*, 419−427.
(3) Sato, O. *Acc. Chem. Res.* **2003**, *36*, 692−700.
(4) Gaspar, A. B.; Ksenofontov, V.; Seredyuk, M.; Gütlich, P. *Coord. Chem. Rev.* **2005**, *249*, 2661−2676.
(5) Bousseksou, A.; Molnár, G.; Salmon, L.; Nicolazzi, W. *Chem. Soc. Rev.* **2011**, *40*, 3313−3335.
(6) Gütlich, P.; Ksenofontov, V.; Gaspar, A. B. *Coord. Chem. Rev.* **2005**, *249*, 1811−1829.
(7) Lyubutin, I. S.; Ovchinnikov, S. G.; Gavriliuk, A. G.; Struzhkin, V. V. *Phys. Rev. B: Condens. Matter Mater. Phys.* **2009**, *79*, 085125.
(8) Wentzcovitch, R. M.; Justo, J. F.; Wu, Z.; da Silva, C. R. S.; Yuen, D. A.; Kohlstedt, D. *Proc. Natl. Acad. Sci. U. S. A.* **2009**, *106*, 8447−8452.
(9) Ohkoshi, S.; Imoto, K.; Tsunobuchi, Y.; Takano, S.; Tokoro, H. *Nat. Chem.* **2011**, *3*, 564−569.
(10) Boldog, I.; Gaspar, A. B.; Martínez, V.; Pardo-Ibañez, P.; Ksenofontov, V.; Bhattacharjee, A.; Gütlich, P.; Real, J. A. *Angew. Chem., Int. Ed.* **2008**, *47*, 6433−6437.
(11) Larionova, J.; Salmon, L.; Guari, Y.; Tokarev, A.; Molvinger, K.; Molnár, G.; Bousseksou, A. *Angew. Chem., Int. Ed.* **2008**, *47*, 8236−8240.
(12) Craig, G. A.; Costa, J. S.; Roubeau, O.; Teat, S. J.; Shepherd, H. J.; Lopes, M.; Molnár, G.; Bousseksou, A.; Aromí, G. *Dalton Trans.* **2014**, *43*, 729−737.
(13) Gaspar, A. B.; Levchenko, G.; Terekhov, S.; Bukin, G.; Valverde-Muñoz, J.; Muñoz-Lara, F. J.; Seredyuk, M.; Real, J. A. *Eur. J. Inorg. Chem.* **2014**, *2014*, 429−433.
(14) Rodríguez-Velamazán, J. A.; Fabelo, O.; Beavers, C. M.; Natividad, E.; Evangelisti, M.; Roubeau, O. *Chem. - Eur. J.* **2014**, *20*, 7956−7961.
(15) Levchenko, G.; Bukin, G. V.; Terekhov, S. A.; Gaspar, A. B.; Martínez, V.; Muñoz, M. C.; Real, J. A. *J. Phys. Chem. B* **2011**, *115*, 8176−8182.
(16) Kantor, I. Y.; Dubrovinsky, L. S.; McCammon, C. A. *Phys. Rev. B: Condens. Matter Mater. Phys.* **2006**, *73*, 100101.
(17) Badro, J.; Struzhkin, V. V.; Shu, J.; Hemley, R. J.; Mao, H.-K. *Phys. Rev. Lett.* **1999**, *83*, 4101−4104.
(18) Lin, J.-F.; Struzhkin, V. V.; Jacobsen, S. D.; Hu, M. Y.; Chow, P.; Kung, J.; Liu, H.; Mao, H.-K.; Hemley, R. J. *Nature* **2005**, *436*, 377−380.
(19) Li, J.; Struzhkin, V. V.; Mao, H.-K.; Shu, J.; Hemley, R. J.; Fei, Y.; Mysen, B.; Dera, P.; Prakapenka, V.; Shen, G. *Proc. Natl. Acad. Sci. U. S. A.* **2004**, *101*, 14027−14030.
(20) Ding, Y.; Haskel, D.; Ovchinnikov, S. G.; Tseng, Y.-C.; Orlov, Y. S.; Lang, J. C.; Mao, H.-K. *Phys. Rev. Lett.* **2008**, *100*, 045508.
(21) Rosner, H.; Koudela, D.; Schwarz, U.; Handstein, A.; Hanfland, M.; Opahle, I.; Koepernik, K.; Kuz'min, M. D.; Müller, K.-H.; Mydosh, J. A.; Richter, M. *Nat. Phys.* **2006**, *2*, 469−472.
(22) Kuneš, J.; Lukoyanov, A. V.; Anisimov, V. I.; Scalettar, R. T.; Pickett, W. E. *Nat. Mater.* **2008**, *7*, 198−202.
(23) Rueff, J.-P.; Kao, C.-C.; Struzhkin, V. V.; Badro, J.; Shu, J.; Hemley, R. J.; Mao, H. K. *Phys. Rev. Lett.* **1999**, *82*, 3284−3287.
(24) Kawakami, T.; Tsujimoto, Y.; Kageyama, H.; Chen, X.-Q.; Fu, C. L.; Tassel, C.; Kitada, A.; Suto, S.; Hirama, K.; Sekiya, Y.; Makino, Y.; Okada, T.; Yagi, T.; Hayashi, N.; Yoshimura, K.; Nasu, S.; Podloucky, R.; Takano, M. *Nat. Chem.* **2009**, *1*, 371−376.
(25) Ming, X.; Meng, X.; Hu, F.; Wang, C.-Z.; Huang, Z.-F.; Fan, H.-G.; Chen, G. *J. Phys.: Condens. Matter* **2009**, *21*, 295902.
(26) Huang, L.; Wang, Y.; Dai, X. *Phys. Rev. B: Condens. Matter Mater. Phys.* **2012**, *85*, 245110.
(27) Javaid, S.; Akhtar, M. J.; Ahmad, I.; Younas, M.; Shah, S. H.; Ahmad, I. *J. Appl. Phys.* **2013**, *114*, 243712.
(28) Adams, D. J.; Amadon, B. *Phys. Rev. B: Condens. Matter Mater. Phys.* **2009**, *79*, 115114.
(29) Hauser, A.; Jeftić, J.; Romstedt, H.; Hinek, R.; Spiering, H. *Coord. Chem. Rev.* **1999**, *190−192*, 471−491.
(30) Real, J. A.; Gaspar, A. B.; Niel, V.; Muñoz, M. C. *Coord. Chem. Rev.* **2003**, *236*, 121−141.
(31) Kimber, S. A. J.; Salamat, A.; Evans, S. R.; Jeschke, H. O.; Muthukumar, K.; Tomić, M.; Salvat-Pujol, F.; Valentí, R.; Kaisheva, M. V.; Zizak, I.; Chatterji, T. *Proc. Natl. Acad. Sci. U. S. A.* **2014**, *111*, 5106−5110.
(32) Xiao, G.; Yang, X.; Zhang, X.; Wang, K.; Huang, X.; Ding, Z.; Ma, Y.; Zou, G.; Zou, B. *J. Am. Chem. Soc.* **2015**, *137*, 10297−10303.
(33) Wang, Y.; Bai, L.; Wen, T.; Yang, L.; Gou, H.; Xiao, Y.; Chow, P.; Pravica, M.; Yang, W.; Zhao, Y. *Angew. Chem., Int. Ed.* **2016**, *55*, 10350−10353.
(34) Mao, H. K.; Xu, J.; Bell, P. M. *J. Geophys. Res.* **1986**, *91*, 4673−4676.
(35) Prescher, C.; Prakapenka, V. B. *High Pressure Res.* **2015**, *35*, 223−230.
(36) Rodriguez-Carvajal, J. *Phys. B* **1993**, *192*, 55−69.
(37) Vankó, G.; Neisius, T.; Molnár, G.; Renz, F.; Kárpáti, S.; Shukla, A.; de Groot, F. M. F. *J. Phys. Chem. B* **2006**, *110*, 11647−11653.
(38) Ouvrard, G.; Brec, R.; Rouxel, J. *Mater. Res. Bull.* **1985**, *20*, 1181−1189.
(39) Wiedenmann, A.; Rossat-Mignod, J.; Louisy, A.; Brec, R.; Rouxel, J. *Solid State Commun.* **1981**, *40*, 1067−1072.
(40) Wildes, A. R.; Kennedy, S. J.; Hicks, T. J. *J. Phys.: Condens. Matter* **1994**, *6*, L335−L341.
(41) Wildes, A. R.; Rønnow, H. M.; Roessli, B.; Harris, M. J.; Godfrey, K. W. *Phys. Rev. B: Condens. Matter Mater. Phys.* **2006**, *74*, 094422.
(42) Sivadas, N.; Daniels, M. W.; Swendsen, R. H.; Okamoto, S.; Xiao, D. *Phys. Rev. B: Condens. Matter Mater. Phys.* **2015**, *91*, 235425.
(43) Joy, P. A.; Vasudevan, S. *J. Am. Chem. Soc.* **1992**, *114*, 7792−7801.
(44) Porras-Montenegro, N.; Duque, C. A. *Phys. E* **2010**, *42*, 1865−1869.
(45) Katrusiak, A.; Szafrański, M.; Podsiadło, M. *Chem. Commun.* **2011**, *47*, 2107−2109.
(46) Xiao, Y. M.; Chow, P.; Boman, G.; Bai, L. G.; Rod, E.; Bommannavar, A.; Kenney-Benson, C.; Sinogeikin, S.; Shen, G. Y. *Rev. Sci. Instrum.* **2015**, *86*, 072206.
(47) Rozenberg, G. Kh.; Xu, W.; Pasternak, M. P. *Z. Kristallogr. - Cryst. Mater.* **2014**, *229*, 210−222.
(48) Xiao, W.; Tan, D.; Xiong, X.; Liu, J.; Xu, J. *Proc. Natl. Acad. Sci. U. S. A.* **2010**, *107*, 14026−14029.
(49) Allen, J. W.; Martin, R. M. *Phys. Rev. Lett.* **1982**, *49*, 1106−1110.
(50) Shannon, R. D. *Acta Crystallogr., Sect. A: Cryst. Phys., Diffr., Theor. Gen. Crystallogr.* **1976**, *A32*, 751−767.

DOI: 10.1021/jacs.6b10225
J. Am. Chem. Soc. 2016, 138, 15751−15757